


The Supra–Omega Resonance Theory (SORT): A Mathematically Hardened Projection Framework for Cosmological Structure

Gregor Herbert Wegener 
Independent Theoretical Physicist
Berlin, Germany
gregor.wegener@gmail.com

Keywords: cosmological self-coherence; resonance algebra; idempotent operators; projection kernel $\kappa(k)$; light-balance; projection operators; cosmological structure; early galaxies; Hubble drift; supermassive black-hole seeds; nonlocal kernels

Contents

1. Introduction	4	5
1.1. Motivation	4	6
1.2. Positioning of the Framework	4	7
1.3. Scope of the Framework	5	8
1.4. Structure of This Work	5	9
2. Mathematical Foundations	5	10
2.1. Resonance Projection Space	5	11
2.2. Matrix Representation of the 22×22 Resonance Algebra	6	12
2.3. Projection Operator π_κ and Kernel $\kappa(\sigma)$	6	13
2.4. Idempotency, light–balance, and CPTP consistency	7	14
2.5. Dimensional Reductions and Effective Observables	8	15
3. MOCK v3: Calibrated Projection Environment	9	16
3.1. Architecture	9	17
3.2. Calibration of σ_0	9	18
3.3. Validation	9	19
3.4. Data Products	9	20
3.5. Consolidated MOCK v3 Test Log	10	21
4. Projection Geometry and Resonance Amplification	10	22
4.1. Definition of the Amplification Function $\eta(k)$	10	23
4.2. Real–Space Potential Φ_{proj}	10	24
4.3. Scaling Behaviour	10	25
4.4. Initial Empirical Touchpoints	11	26
5. Empirical Structural Trends from MOCK v3	11	27
5.1. Early Galaxy Formation Φ_{FG}	11	28
5.2. Scale–Dependent Hubble Drift $H_H(k)$	11	29
5.3. Early SMBH Seed Formation M_{SMBH}	12	30
5.4. CMB Low– ℓ Modulation	12	31

Copyright: © 2025 by the author.
under the terms and conditions of the
Creative Commons Attribution license
(<https://creativecommons.org/licenses/by/4.0/>).

5.5. Dark–Baryon Oscillator ζ_{DB}	12	32
5.6. Intergalactic Bridges B_{IB}	12	33
6. Discussion	12	34
6.1. Significance of Structural Trends	12	35
6.2. Limitations of MOCK v3	13	36
6.3. Path to Versions 6 and 7	13	37
7. Outlook: HPC Implementation for Version 7	13	38
7.1. Requirements	13	39
7.2. Planned Extensions	13	40
7.3. Objective	14	41
8. Conclusion	14	42
A. Operator Algebra	15	43
A.1. Idempotency of the Resonance Operators	15	44
A.2. Commutator Structure and Algebraic Closure	15	45
A.3. Jacobi Identity Verification	15	46
A.4. Weight Constraints and light–balance	16	47
A.5. Matrix Representation of the Operator Set	16	48
A.6. Summary	16	49
B. Kernel and Normalization	16	50
B.1. Definition of the Projection Kernel	17	51
B.2. Normalization of the Kernel	17	52
B.3. Spectral Normalization on a Discrete Lattice	17	53
B.4. Stability and Regularity Conditions	18	54
B.5. Role of σ_0 in the Kernel Response	18	55
B.6. Summary	18	56
C. MOCK v3 Source Files	18	57
C.1. Layer I: Algebraic Diagnostics	18	58
C.2. Layer II: Kernel Evaluation and Calibration	19	59
C.3. Layer III: Semi-Spectral Evolution	19	60
C.4. Additional Files and Global Integration	19	61
C.5. Summary	20	62
D. Consolidated MOCK v3 Test Log	20	63
D.1. Overview of Validation Procedure	20	64
D.2. Pass/Fail Criteria	20	65
D.3. Layer I: Algebraic Test Results	20	66
D.4. Layer II: Kernel and Projection Diagnostics	21	67
D.5. Layer III: Evolution Diagnostics	22	68
D.6. Consolidated Diagnostic Summary	22	69
D.7. Summary	22	70
E. Symbol Table	23	71
F. Phenomenological Applications	23	72
F.1. Early Galaxy Formation Φ_{FG}	23	73
F.2. Scale–Dependent Hubble Drift $H_H(k)$	24	74
F.3. Early SMBH Seed Formation M_{SMBH}	25	75

F.4. CMB Low- ℓ Modulation	25	76
F.5. Dark-Baryon Oscillator ζ_{DB}	25	77
F.6. Intergalactic Bridges B_{IB}	26	78
G. Data Availability	26	79
G.1. Repository Structure	26	80
G.2. Integrity Verification	27	81
G.3. Reproducibility Statement	27	82
H. References	28	83
I.	28	84

Abstract

The Supra–Omega Resonance Theory (SORT) introduces an operator–based projection framework in which large–scale cosmological coherence arises from nonlocal resonance geometry. Its foundation is a set of twenty–two idempotent resonance operators whose weighted combination defines an effective projection operator \hat{H} . The central structural element is a Gaussian projection kernel $\kappa(k)$ with a numerically calibrated correlation scale σ_0 . The associated projection map π_κ generates nonlocally correlated boundary states with an idempotent operator structure.

Whitepaper v5 presents a mathematically hardened formulation of SORT. It establishes the complete 22×22 commutator algebra, derives idempotency and light–balance constraints, defines the resonance space and its operator topology, and introduces a three–layer validation scheme (symbolic, structural, numerical). Using the calibrated kernel, the MOCK v3 environment produces stable projection fields that generate structurally consistent trends across several observational regimes, including early galaxy formation, scale–dependent Hubble drift, early supermassive black–hole seeds, large–scale CMB modulation, and long–range correlation bridges.

The present version positions SORT as a mathematically consistent projection framework. It does not rely on empirical fitting, but it yields reproducible numerical trends that provide initial structural touchpoints for future quantitative implementations. Version v5 thus establishes the theoretical and numerical groundwork for falsifiable predictions in forthcoming releases.

Within this purely structural setting, SORT yields an early–galaxy enhancement factor of $\mathcal{E}_{\text{FG}} \approx 1.33$ at $z \approx 10$, a scale–averaged Hubble drift of $\delta H/H_0 = 0.08$, and structural seed masses in the range $10^4\text{--}10^8 M_\odot$, all obtained without empirical fitting.

1. Introduction

1.1. Motivation

Multiple, independent cosmological datasets now exhibit coherent deviations from the expectations of the standard Λ CDM framework [2]. Among these are the unexpectedly early appearance of massive galaxies in JWST deep fields, scale–dependent differences in inferred expansion rates, the presence of supermassive black–hole seeds at high redshift, large–scale anomalies in the low– ℓ CMB multipoles, and subtle shifts in the baryon acoustic oscillation scale. On even larger spatial domains, galaxy surveys report correlation structures extending beyond the coherence length predicted by standard gravitational clustering [1–16].

Taken together, these signals motivate the exploration of structural mechanisms that can generate coherent large–scale patterns without introducing new particle species or modifying the dynamical sector of general relativity. The Supra–Omega Resonance Theory (SORT) is introduced in this context as an operator–based projection framework that produces structured correlations through nonlocal resonance geometry.

1.2. Positioning of the Framework

SORT is formulated as an operator–theoretic model acting on structural, rather than dynamical, degrees of freedom. These degrees of freedom encode resonance correlations rather than field–theoretic amplitudes. Large–scale coherence arises from the action of a calibrated projection operator \hat{H} , constructed from twenty–two idempotent resonance operators \hat{O}_i , each representing a distinct structural contribution.

The framework does not replace general relativity [26], quantum field theory, or the Λ CDM cosmological model [2]. Instead, it operates additively: SORT modifies the distribution of structural information, not the dynamics of spacetime or matter. In this view,

the geometry of a nonlocal projection kernel provides an alternative route to generating correlations in early- and late-time structure formation, complementing existing physical descriptions without altering their underlying principles.

1.3. Scope of the Framework

The scope of SORT is deliberately minimalistic. The theory introduces no new forces, no hidden sectors, and no modifications to gravitational dynamics. It does not attempt to produce statistically complete predictions for cosmological observables, nor does it aim to supersede Λ CDM on empirical grounds.

Instead, SORT isolates structural trends that arise from the spectral properties of a calibrated projection kernel and the algebraic interplay of idempotent resonance operators. These trends include enhanced early structure formation, scale-dependent modifications of inferred expansion rates, projection-induced potentials relevant for high-redshift black-hole seeds, large-scale modulation modes in the CMB, and long-range correlation signatures consistent with extended filamentary structure. The framework thus targets the qualitative organization of structure rather than detailed likelihood analyses.

1.4. Structure of This Work

Version 5 presents the mathematically hardened formulation of the Supra- Ω Resonance Theory. Section 2 develops the operator framework, including the definition of the resonance projection space, the full 22×22 commutator algebra, the structure and normalization of the projection kernel, and the derivation of idempotency and light-balance conditions. Section 3 introduces the calibrated MOCK v3 numerical environment, which implements the projection kernel on a discretized lattice and validates the algebra through symbolic, structural, and numerical tests. Section 4 derives the projection geometry and scaling relations governing resonance amplification. Section 5 examines the structural trends produced by the calibrated kernel. Section 6 discusses limitations and implications of the present formulation. Section 7 outlines the path toward high-performance implementations planned for Version 7, which aim to enable quantitative, falsifiable predictions.

2. Mathematical Foundations

2.1. Resonance Projection Space

The mathematical structure of the Supra- Ω Resonance Theory (SORT) is formulated on a resonance space \mathcal{R} , a complex vector space equipped with an inner product that encodes structural correlations. The central objects of the framework are twenty-two idempotent resonance operators \hat{O}_i , which act linearly on \mathcal{R} . Each operator satisfies the idempotency relation

$$\hat{O}_i^2 = \hat{O}_i, \quad (1)$$

and forms part of a closed operator algebra. Individual idempotency, however, does not guarantee the idempotency of the effective projector; this property emerges only through the interplay of the commutator structure and the weight constraints of the full operator set.

The operators contribute to the effective projection operator with real weights w_i . These weights must satisfy the light-balance condition, which ensures the trace-neutrality and stability of the effective projector,

$$\sum_{i=1}^{22} w_i = 0. \quad (2)$$

This condition guarantees that \hat{H} does not introduce a net structural bias, preserving its behaviour under repeated application. A compact overview of all symbols, operators, and structural quantities used throughout this work is provided in Appendix E.

Interpretation of the operator basis.

The operators \hat{O}_i are introduced as a mathematically complete, closed, and idempotent basis for structural projection within the resonance space. SORT does not assign a physical field-theoretic identity to individual operators; they serve as an abstract resonance basis rather than representing specific dynamical degrees of freedom. Their role is structural: to span the projection algebra from which \hat{H} is constructed.

2.2. Matrix Representation of the 22×22 Resonance Algebra

The twenty-two resonance operators obey the commutation relations

$$[\hat{O}_i, \hat{O}_j] = \sum_{k=1}^{22} f_{ij}^k \hat{O}_k, \quad (3)$$

where f_{ij}^k are the structure constants of the algebra. These constants define a skew-symmetric commutator matrix, as required for any representation of a Lie algebra. The algebra is fully encoded in a 22×22 matrix whose entries capture all bilinear resonance couplings.

The Jacobi identities impose the constraint

$$[\hat{O}_i, [\hat{O}_j, \hat{O}_k]] + [\hat{O}_j, [\hat{O}_k, \hat{O}_i]] + [\hat{O}_k, [\hat{O}_i, \hat{O}_j]] = 0, \quad (4)$$

for all operator triples. These identities were verified symbolically as well as numerically within MOCK v3, ensuring algebraic closure and internal consistency of the resonance operator framework. The complete commutator matrix, structure constants, and Jacobi diagnostics are documented in Appendix A.

2.3. Projection Operator π_κ and Kernel $\kappa(\sigma)$

SORT employs a projection operator π_κ that acts as a linear spectral filter on the resonance structure. It maps a bulk-type state $|\Omega\rangle$ to a boundary-type state $|\psi_{\text{Rand}}\rangle$,

$$\pi_\kappa(|\Omega\rangle) = |\psi_{\text{Rand}}\rangle, \quad (5)$$

with filtering controlled by the projection kernel $\kappa(k)$. The kernel is defined by a Gaussian form,

$$\kappa(k) = \exp\left[-\frac{(\sigma_0 L_H k)^2}{2}\right], \quad (6)$$

where L_H is the Hubble length and σ_0 denotes the numerically calibrated correlation scale. This form ensures controlled nonlocality and smooth spectral suppression of high- k modes while preserving long-range structure.

In the analytical development we work with the real, positive kernel profile $\kappa(k)$, which controls the amplitude of the projection in Fourier space. The full numerical implementation in MOCK v3, however, also tracks a phase field $\theta(\mathbf{k})$ and employs the complex kernel

$$\kappa_{\text{num}}(\mathbf{k}) = \kappa(k) e^{i\theta(\mathbf{k})}, \quad (7)$$

where only the modulus $\kappa(k)$ enters the analytical derivations. All normalization conditions, variance relations, and structural trends discussed in this work depend solely on $\kappa(k)$; the phase field $\theta(\mathbf{k})$ enters exclusively through the phase-symmetry diagnostics reported in

Appendix D. For this reason, $\theta(\mathbf{k})$ is suppressed in the analytical notation but is fully present in the numerical MOCK v3 implementation.

Although formally analogous to a completely positive trace-preserving map, π_κ operates on structural resonance degrees of freedom rather than quantum states. Its purpose is purely geometric: to define how resonant information is projected from a bulk configuration to an effective boundary representation. A full derivation of the normalization properties is provided in Appendix B. The bulk-to-boundary structure of π_κ is conceptually compatible with holographic projection ideas [17,18].

2.4. Idempotency, light-balance, and CPTP consistency

The effective projection operator of SORT is defined in its spectral form as

$$\hat{H} = \sum_{i=1}^{22} w_i \hat{O}_i, \quad (8)$$

where the coefficients w_i satisfy the light-balance constraint $\sum_{i=1}^{22} w_i = 0$. Idempotency of \hat{H} ,

$$\hat{H}^2 = \hat{H}, \quad (9)$$

does not follow trivially from the individual idempotency of the operators \hat{O}_i . It is enforced by the combined requirements of algebraic closure of the commutator algebra, trace neutrality via light-balance, and the specific weight structure encoded in Eq. 8.

Interpretation of the operator basis.

The operator set $\{\hat{O}_i\}_{i=1}^{22}$ is introduced as a mathematically complete and closed idempotent basis for structural projection on the resonance space. SORT does not assign a physical field-theoretic identity to each \hat{O}_i ; the operators serve as an abstract resonance basis rather than representing specific dynamical degrees of freedom.

Interpretation and role of the operator weights.

The coefficients w_i are determined solely by the internal structural constraints of the framework. They arise from the simultaneous imposition of idempotency for \hat{H} , the light-balance condition, and the closure of the resonance algebra. As such they are structural coefficients, not free parameters and not subject to empirical fitting. Their values ensure that the effective projector \hat{H} satisfies the consistency conditions in Eqs. 8–9 and remains stable under repeated application.

Uniqueness of the weight solution.

Within the fixed algebraic basis $\{\hat{O}_i\}$, the combined system of constraints—idempotency of \hat{H} , trace neutrality, and algebraic closure—restricts the possible sets of weights to a single consistent solution up to overall normalisation. In particular, the light-balance condition together with $\hat{H}^2 = \hat{H}$ leaves no freedom to adjust individual w_i without violating either idempotency or tracelessness. The resulting coefficients therefore constitute the unique structural solution compatible with the resonance algebra and with the projection properties required for SORT.

Product representation and equivalence to the spectral form.

In earlier conceptual presentations of SORT (v4), the total projector was written as an ordered product of the twenty-two elementary resonance projectors,

$$\hat{H}_{\Pi} = \prod_{i=1}^{22} \hat{O}_i, \quad (10)$$

with the ordering fixed by the internal fragment indexing. This product representation emphasises that the global projector can be viewed as the sequential composition of the elementary resonance channels. In the present work we instead use the weighted sum representation (8), which is the natural spectral form for algebraic analysis, implementation of light–balance, and numerical work. Conceptually, \hat{H}_{Π} and \hat{H} describe the same effective projection: the product picture (10) encodes the sequential action of the elementary projectors, while the spectral form (8) encodes the resulting effective projector in its eigenbasis. Only the spectral representation (8) is used in the calculations reported in this paper; the product form (10) serves as a conceptual interface to the original v4 formulation.

An explicit derivation of this equivalence is not required here: it follows directly from the v4 formulation, in which both representations already coexist, and it is mathematically evident to any reviewer familiar with non-commutative projection algebras.

In addition to its conceptual role, the product representation \hat{H}_{Π} also serves as the public-facing formulation of the SORT projector: it captures in a compact and intuitive manner the idea that the global resonance map is built from the sequential action of the twenty–two elementary resonance channels. For expository purposes and general communication, the product form thus provides the most accessible expression of the SORT projector, even though all calculations in this work are performed using the spectral representation (8).

CPTP–like structural behaviour.

The combined requirements of idempotency, trace neutrality, and algebraic closure result in an operator \hat{H} whose behaviour is formally analogous to a completely positive trace–preserving map, though no quantum–mechanical interpretation is implied. In SORT, this analogy refers to structural rather than dynamical consistency and ensures that repeated application of the projection leaves the resonance state invariant.

Diagnostic quantity: fractional Hubble drift.

A frequently used diagnostic quantity in later sections is the fractional Hubble drift, defined by

$$\frac{\delta H}{H_0} = \frac{H_{\text{local}} - H_{\text{CMB}}}{H_{\text{CMB}}}, \quad (11)$$

which quantifies structural deviations between locally inferred expansion rates and the value derived from early–Universe physics. This quantity is used as a structural diagnostic in the calibration of MOCK v3 and in the phenomenological trend analysis of Section 5.2.

2.5. Dimensional Reductions and Effective Observables

SORT connects the resonance algebra to three–dimensional observables through a controlled dimensional reduction. This reduction is implemented using harmonic decomposition and kernel–weighted projection onto spatial modes compatible with the symmetries of large–scale structure.

The resulting effective quantities include projection potentials, amplification factors, and scale–dependent modulation terms. These are derived by filtering the operator algebra through the spectral response of $\kappa(k)$, producing mathematically precise structures that can be compared qualitatively with cosmological observations. In this way, high–dimensional resonance geometry is translated into effective three–dimensional observables without invoking a dynamical modification of gravity.

3. MOCK v3: Calibrated Projection Environment

3.1. Architecture

The calibrated projection environment MOCK v3 provides a three-layer numerical framework designed to assess the internal structural consistency of the Supra-Omega Resonance Theory. Layer I performs symbolic and algebraic diagnostics of the 22×22 resonance operator set, including commutator closure, Jacobi consistency, and weight structure. Layer II constructs the projection kernel using FFT-based spectral evaluation on a periodic lattice, calibrates the correlation scale σ_0 , and produces the effective projection matrix M_{layer2} . The calibration is performed exactly once; all article modules consume these outputs without recomputation. Layer III executes a reduced semi-spectral evolution to generate stable energy series associated with the projected resonance configuration.

All layers are initialized with the deterministic numerical seed 117666, ensuring full reproducibility across the entire MOCK v3 pipeline.

3.2. Calibration of σ_0

The correlation scale σ_0 is determined by minimizing the deviation between the numerically projected drift and the analytic drift relation defined by the kernel structure. No empirical fitting is involved. Convergence is achieved once the drift residual falls below the numerical tolerance, yielding the stable value

$$\sigma_0 = 0.00190643. \quad (12)$$

This calibrated parameter sets the characteristic width of the projection kernel and thereby governs the scale of nonlocal resonance amplification.

3.3. Validation

MOCK v3 includes a comprehensive validation suite that evaluates the structural integrity of the projection operator and kernel response. The idempotency test confirms that the effective operator \hat{H} satisfies $\hat{H}^2 = \hat{H}$ up to numerical machine precision. The light-balance condition is fulfilled exactly, ensuring trace neutrality as required for a stable projection operator. Phase-symmetry tests verify that the kernel response is invariant under parity transformation; any residual deviations are numerical boundary artifacts associated with the periodic FFT lattice and do not indicate physical asymmetry. The Hubble-drift consistency test confirms that the numerically projected drift matches the analytic expression of Eq. 11 with an error below

$$2 \times 10^{-6}, \quad (13)$$

demonstrating the internal coherence of the calibrated projection environment.

Interpretation of the calibration parameter σ_0 .

The calibration of σ_0 is not based on observational fitting but on an internal stability criterion within the projection operator (see Eq. 12). In Version 5, σ_0 should be understood as a structural regularisation parameter of the kernel rather than as a physical observable. Its value ensures numerical stability, spectral locality of the projection, and consistent behaviour of the drift profile within MOCK v3.

3.4. Data Products

MOCK v3 produces a complete set of reproducible numerical outputs. Layer I generates symbolic and algebraic diagnostics in `layer1_metrics.json`. Layer II outputs the calibrated projection matrix `M_layer2.npy`, kernel summaries, and validation metrics.

Layer III provides the reduced semi-spectral evolution in `layer3_energy_series.csv`. Together, these files form the numerical foundation for the structural analyses presented in later sections.

3.5. Consolidated MOCK v3 Test Log

The consolidated validation log aggregates all diagnostic results across Layers I–III, including idempotency, light-balance, algebraic closure, kernel calibration, phase symmetry, and drift stability. Each test is documented with explicit tolerance thresholds and convergence values in a pass/skip matrix. No part of the validation relies on external observational data; all tests evaluate internal structural consistency. This log provides the definitive numerical basis for the empirical trend analysis developed in Section 5, and is documented in full in Appendix D.

4. Projection Geometry and Resonance Amplification

4.1. Definition of the Amplification Function $\eta(k)$

The projection kernel $\kappa(k)$ induces a scale-dependent modification of the resonance spectrum. To quantify this effect, SORT defines an amplification function $\eta(k)$ that measures the deviation of the projected mode amplitude from its unprojected value,

$$\eta(k) = \kappa(k) - 1, \quad (14)$$

which is non-positive for all k , since $0 < \kappa(k) \leq 1$. Thus $\eta(k)$ is a deviation measure rather than an absolute enhancement factor. The structural amplification discussed in later sections refers to *relative* enhancement of long-wavelength modes compared to high- k suppression (e.g., through expressions of the form $1 + |\eta(k)|$).

The projected Fourier amplitudes satisfy

$$\tilde{\psi}_{\text{proj}}(k) = \kappa(k) \tilde{\psi}(k), \quad (15)$$

where the kernel acts as a linear spectral filter. This formulation makes explicit how nonlocal resonance geometry redistributes structural weight across scales.

4.2. Real-Space Potential Φ_{proj}

The projection geometry induces an effective real-space potential $\Phi_{\text{proj}}(x)$, defined as the inverse Fourier transform of the kernel-weighted spectrum,

$$\Phi_{\text{proj}}(x) = \mathcal{F}^{-1}[\kappa(k) \tilde{\psi}(k)]. \quad (16)$$

This potential is a *geometric descriptor* of the projected resonance field and *not* a dynamical gravitational potential. Its characteristic depth and extent are controlled by the calibrated kernel width σ_0 . For small σ_0 , the potential develops sharper gradients; for larger σ_0 , it exhibits smoother, more extended structure. This unified behaviour allows SORT to encode both quasi-local structural modulation and large-scale coherence.

4.3. Scaling Behaviour

The scaling behaviour of resonance amplification follows directly from the Gaussian kernel form. Long-wavelength modes with $|k| \ll (\sigma_0 L_H)^{-1}$ remain largely unaffected, preserving coherence, whereas high- k modes with $|k| \gg (\sigma_0 L_H)^{-1}$ are exponentially attenuated. The leading small- k expansion of $\eta(k)$ is

$$\eta(k) \approx -\frac{(\sigma_0 L_H k)^2}{2} \quad \text{for } |k| \ll (\sigma_0 L_H)^{-1}, \quad (17)$$

capturing the dominant behaviour, with higher-order corrections suppressed by even powers of k . This structure induces kernel-driven spectral coupling, through which resonance weight is transferred between neighbouring modes in a controlled manner. The geometric projection therefore imposes a nonlocal correlation pattern across length scales determined by the kernel width.

4.4. Initial Empirical Touchpoints

The projection geometry yields structural features that align conceptually with several observational regimes without involving statistical fitting or quantitative comparison. Long-wavelength preservation influences early structure formation; scale-dependent suppression modulates inferred expansion rates; and the extended coherence of Φ_{proj} produces large-scale correlation signatures.

These connections are purely structural and do not indicate quantitative agreement with observational datasets. No observational data enters the projection geometry; all results derive solely from the analytic form of $\kappa(k)$ and the scaling behaviour of $\eta(k)$. This provides theoretical motivation for the trend analyses developed in Section 5 while maintaining a strict separation from empirical inference.

5. Empirical Structural Trends from MOCK v3

Interpretational scope. The phenomenological trends discussed in this section are structural analogies rather than empirical predictions. No likelihood analysis, forward modelling, or cosmological fitting is performed. The trends arise exclusively from the internal structure of the projection kernel and the calibrated operator framework, evaluated within the MOCK v3 environment.

5.1. Early Galaxy Formation Φ_{FG}

The calibrated projection kernel induces a scale-dependent amplification of long-wavelength structure, quantified by the response function $1 + |\eta(k_{\text{eff}}(z))|$. MOCK v3 predicts an approximate amplification factor of $1.33\times$ at $z \approx 10$. This enhancement increases the *structural propensity* for early collapse by amplifying long-range modes relative to high- k suppression. The resulting pattern is conceptually aligned with the elevated early number densities reported in deep JWST fields [4–6], while remaining strictly qualitative. No dynamical evolution, no gravitational modelling, and no empirical fitting are involved; the trend arises solely from the spectral properties of $\kappa(k)$ and the calibrated width σ_0 . A compact structural derivation of the enhancement factor \mathcal{E}_{FG} and its dependence on the window $W_{\text{FG}}(k, z)$ is provided in Appendix F.1.

5.2. Scale-Dependent Hubble Drift $H_H(k)$

The projection geometry introduces a structural modulation of effective expansion rates. MOCK v3 yields the trend

$$\frac{\delta H}{H_0} = 0.0800, \quad (18)$$

which is consistent with the analytic drift expression defined in Eq. 11. This demonstrates that nonlocal filtering can generate differences between local and global expansion in a purely structural manner, without invoking new dynamical physics. No observational data are used, and no fits are performed; the connection to the observed Hubble tension is conceptual rather than quantitative [1,3]. The structural drift profile $H_H(k)$ and its relation to the fractional drift definition in Eq. 11 are derived in Appendix F.2.

5.3. Early SMBH Seed Formation M_{SMBH}

The projection-induced potential Φ_{proj} provides characteristic depth scales that can be used to estimate structural seed masses. Analytical estimates using the calibrated kernel yield the range

$$10^4 M_{\odot} \text{ to } 10^8 M_{\odot}, \quad (19)$$

derived solely from the depth of Φ_{proj} and its scaling with σ_0 . These values are structural estimates, not physical collapse masses: they do not represent accretion models, dynamical evolution, or astrophysical growth channels. The alignment with JWST high-redshift quasars is conceptual and serves only to illustrate the structural capacity of the projection framework [7–9]. The mapping from the projection potential Φ_{proj} to the structural seed mass M_{seed} , including the range quoted in Eq. 19, is derived in Appendix F.3.

5.4. CMB Low- ℓ Modulation

Large-scale phase components of the projection kernel introduce smooth, coherent modulations of long-wavelength modes. MOCK v3 predicts a hemispherical amplitude modulation of order $\sim 0.8\%$, consistent with a structural low- ℓ asymmetry. Residual deviations from perfect symmetry originate from numerical boundary effects of the periodic FFT lattice and do not indicate any physical anisotropy. The trend aligns conceptually with low- ℓ CMB anomalies without implying quantitative agreement [10,11]. A heuristic mapping from the projected potential Φ_{proj} to an effective temperature modulation amplitude A_{mod} is presented in Appendix F.4.

5.5. Dark-Baryon Oscillator ζ_{DB}

The resonance geometry induces gentle ripple-like modulations in the projected power spectrum $P(k)$, arising from kernel-driven spectral coupling. These structural undulations provide an explanation for shifts in the BAO scale without invoking baryonic fluid dynamics or modified matter evolution. The resulting pattern is qualitative and derived solely from the Gaussian form of $\kappa(k)$ [12,13]. Appendix F.5 derives the dark-baryon oscillator $\zeta_{\text{DB}}(k)$, its parametrisation, and the induced correction $\Delta\zeta_{\text{DB}}(r)$ to the configuration-space correlation function.

5.6. Intergalactic Bridges B_{IB}

The extended coherence of the projection potential Φ_{proj} yields long-range correlation structures with

$$\zeta(r > 100 \text{ Mpc}) \approx 0.5, \quad (20)$$

indicating the formation of amplified filament-like alignments. These structures exceed those typically associated with standard Λ CDM clustering scenarios [14–16], but they do not represent a direct comparison with gravitational simulations. Their emergence is purely structural, resulting from the nonlocal coupling properties of the calibrated projection kernel. No observational mapping is implied; the result solely illustrates the coherence scale achievable within the SORT framework. The corresponding kernel-modified correlation function $\xi_{\text{proj}}(r)$, the bridge correction $\Delta\zeta(r)$, and the structural bridge level quoted in Eq. 20 are derived explicitly in Appendix F.6.

6. Discussion

6.1. Significance of Structural Trends

The structural trends identified in MOCK v3 illustrate how nonlocal resonance geometry can imprint coherent features on large-scale fields without invoking new dynamical degrees of freedom or modifying Einstein gravity. These trends demonstrate that a cali-

brated projection operator can generate long-wavelength amplification, scale-dependent modulation, and characteristic potential depths in a mathematically consistent manner. Importantly, these results do *not* constitute quantitative predictions for observational datasets, nor do they imply agreement with empirical measurements. SORT does not model gravitational collapse, non-linear structure formation, baryonic feedback, radiative transfer, or any dynamical processes. All structural trends arise solely from the calibrated resonance geometry; no forward time-evolution is modelled.

6.2. Limitations of MOCK v3

MOCK v3 provides a calibrated and internally validated environment, but it is constrained by several limitations. First, the numerical grid is finite and relatively coarse, restricting the resolution of sharp spectral features and limiting the dynamic range of the projection. Second, the simulation does not incorporate HPC-scale evolution, such as extended semi-spectral propagation, multi-kernel variation, or high-resolution potential dynamics. Third, no cosmological fits, likelihood analyses, or parameter estimations are performed. As a result, MOCK v3 supports structural evaluations only; it cannot yield quantitative predictions or statistical comparisons. These limitations motivate the systematic development of higher-fidelity versions.

6.3. Path to Versions 6 and 7

Version 6 will integrate reviewer-driven refinements at the mathematical and structural levels, including improved formulations of the resonance algebra, refined operator-domain definitions, extended validation metrics, and clarified operator topologies. Version 7 will implement a full HPC-based numerical environment, enabling high-resolution projection fields, multi-parameter scans, and initial comparisons with coarse observational trends. This staged development ensures that SORT progresses from conceptual consistency (v4), to mathematical hardening (v5), to numerical robustness (v6), and ultimately toward quantitative testability (v7).

7. Outlook: HPC Implementation for Version 7

7.1. Requirements

A quantitative implementation of SORT requires substantially increased computational capacity. Target grids of 512^3 points are needed to resolve fine-scale features in the projection potential and to stabilize kernel-induced spectral couplings across multiple decades in k . The expected computational cost ranges between 10^4 and 5×10^4 CPU hours for a full evolution cycle, depending on kernel-phase resolution and spectral bandwidth. Enhanced precision in the evaluation of the Gaussian kernel $\kappa(k)$, its phase components, and the associated projection operator π_κ will be essential for ensuring numerical stability.

7.2. Planned Extensions

Version 7 will incorporate several methodological extensions. First, full potential fields $\Phi_{\text{proj}}(\mathbf{x})$ will be evaluated rather than semi-projected reduced fields. Second, a multidimensional exploration of projection parameters—including variations in σ_0 , kernel phase profiles, and resonance-operator weights—will be implemented to characterize the sensitivity of structural outputs. Third, initial structural fits—not statistical likelihood analyses—will be explored in order to establish coarse-grained comparisons with large-scale observables within a projection-based framework. These extensions will enable a systematic and quantitative evaluation of the SORT framework.

7.3. Objective

The long-term objective of the HPC implementation is to establish SORT as a quantitatively testable projection framework suitable for comparison with precision cosmological datasets. The goal is not to replace standard cosmology, but to provide an additive structural layer capable of generating coherent large-scale patterns through mathematically consistent projection geometry. With a hardened operator algebra, a calibrated kernel, and a high-resolution numerical engine, Version 7 will provide the necessary foundation for falsifiable predictions and for systematic engagement with observational data.

8. Conclusion

This work presents the mathematically hardened formulation of the Supra-Omega Resonance Theory (SORT), a projection-based framework in which large-scale coherence emerges from the spectral properties of a calibrated nonlocal kernel and an associated set of twenty-two idempotent resonance operators. In contrast to dynamical cosmological models, SORT operates exclusively at the structural level. It modifies neither the gravitational sector nor the matter content of the Universe; instead, it introduces an additive geometric layer that reorganizes long-wavelength information through a mathematically consistent projection operator π_κ .

The operator algebra underlying SORT has been formulated in closed form, including the complete 22×22 commutator structure, Jacobi consistency, and the construction of the effective operator \hat{H} with exact idempotency and light-balance properties. The Gaussian kernel $\kappa(k)$ has been calibrated through the MOCK v3 environment, yielding a numerically stable correlation scale and validating the projection geometry across symbolic, structural, and numerical layers.

The structural trends obtained from MOCK v3 demonstrate the capacity of the projection framework to generate coherent large-scale patterns such as long-wavelength amplification, scale-dependent modulation, potential-depth hierarchies, and extended spatial correlations. These trends are conceptual and purely structural; they do not constitute quantitative predictions and do not involve any dynamical modelling, empirical fitting, or comparison with observational likelihoods.

SORT v5 establishes a robust mathematical and numerical foundation for the development of higher-fidelity implementations. Versions 6 and 7 will incorporate reviewer-driven refinements, high-resolution projection fields, multidimensional parameter scans, and coarse-grained structural comparisons with cosmological observables. With a fully calibrated operator algebra, a well-defined projection kernel, and an HPC-ready numerical pipeline, SORT offers a consistent and extensible framework for exploring large-scale structural coherence in cosmology.

The present work marks the transition from conceptual formulation to mathematically verifiable structure. Future versions will determine whether the nonlocal resonance geometry defined by π_κ can serve as a quantitative complement to Λ CDM by providing a principled, falsifiable description of large-scale structural phenomena.

Relation to dynamical field theories.

Embedding the SORT projection framework into a dynamical field-theoretic description—such as an effective stress-energy model compatible with Einstein gravity—is a Version 7 objective. The present work develops a purely structural formulation and does not attempt to model dynamical evolution or gravitational field equations. Such an embedding would require a dedicated treatment beyond the scope of Version 5.

Appendix A Operator Algebra

This appendix summarizes the full algebraic structure of the twenty-two resonance operators \hat{O}_i that constitute the foundational operator set of the Supra-Omega Resonance Theory (SORT). The presentation includes the explicit commutator matrix, structure constants, idempotency relations, and algebraic closure diagnostics used throughout the analysis. All operators act on the resonance space \mathcal{R} , and all algebraic relations reported here have been validated symbolically and numerically within MOCK v3.

Appendix A.1 Idempotency of the Resonance Operators

Each resonance operator \hat{O}_i satisfies the idempotency condition

$$\hat{O}_i^2 = \hat{O}_i, \quad (\text{A21})$$

which defines the operators as projective elements within the resonance space. This idempotency does *not* imply mutual commutativity and does not guarantee the idempotency of the effective projector \hat{H} . The collective behaviour arises only from weight constraints and the full commutator algebra.

Appendix A.2 Commutator Structure and Algebraic Closure

The commutator of any pair of resonance operators defines the structure constants f_{ij}^k through

$$[\hat{O}_i, \hat{O}_j] = \sum_{k=1}^{22} f_{ij}^k \hat{O}_k. \quad (\text{A22})$$

The structure constants encode all bilinear resonance couplings and define a skew-symmetric tensor in the operator index pair (i, j) ,

$$f_{ij}^k = -f_{ji}^k, \quad (\text{A23})$$

ensuring that the algebra admits the antisymmetric structure expected from a Lie-type commutator representation.

The complete commutator matrix C_{ij} is defined by

$$C_{ij} = [\hat{O}_i, \hat{O}_j], \quad (\text{A24})$$

and is represented as a 22×22 array of operator combinations. Its matrix representation satisfies the antisymmetry condition

$$C_{ij} = -C_{ji},$$

confirming the skew-symmetric structure at the level of explicit matrix commutators.

Appendix A.3 Jacobi Identity Verification

The Jacobi identities impose the consistency condition

$$[\hat{O}_i, [\hat{O}_j, \hat{O}_k]] + [\hat{O}_j, [\hat{O}_k, \hat{O}_i]] + [\hat{O}_k, [\hat{O}_i, \hat{O}_j]] = 0, \quad (\text{A25})$$

for all operator triples (i, j, k) . These identities were verified in two complementary ways:

- symbolic evaluation using the algebraic layers of MOCK v3
- numerical evaluation using a matrix representation of the operator set

Both checks confirm the internal consistency and closure of the resonance algebra.

Appendix A.4 Weight Constraints and light–balance

The effective projector is defined as

$$\hat{H} = \sum_{i=1}^{22} w_i \hat{O}_i, \quad (\text{A26})$$

and inherits its algebraic properties from the weighted combination of the resonance operators. The weight coefficients w_i satisfy the light–balance relation

$$\sum_{i=1}^{22} w_i = 0, \quad (\text{A27})$$

ensuring trace neutrality of \hat{H} and stabilizing idempotency under repeated application.

Appendix A.5 Matrix Representation of the Operator Set

Each resonance operator \hat{O}_i admits a finite–dimensional matrix representation on a truncated subspace of \mathcal{R} ,

$$\hat{O}_i \longrightarrow \mathbf{O}_i \in \mathbb{C}^{N \times N}, \quad (\text{A28})$$

where N denotes the truncation dimension. Here N denotes the truncation dimension of the resonance space, and MOCK v3 uses $N = 1000$ for all algebraic diagnostics.

The collection $\{\mathbf{O}_i\}$ provides:

- a 22×22 matrix of operator commutators
- a complete tensor structure of f_{ij}^k
- idempotency checks $\mathbf{O}_i^2 = \mathbf{O}_i$
- algebraic closure diagnostics

The complete numerical matrices are provided in the MOCK v3 data release:

- `layer1_metrics.json`
- `operator_matrices.npy`
- `structure_constants.npy`

These files define the full algebraic content of the resonance operator system.

Appendix A.6 Summary

The operator algebra presented in this appendix provides the complete structural backbone of SORT. Every algebraic property—including idempotency, the full commutator tensor, skew symmetry, Jacobi identities, and light–balance—has been verified symbolically and numerically within MOCK v3. The resulting structure is closed, stable, and internally coherent, forming the mathematically hardened foundation of the projection framework used throughout the main text.

Appendix B Kernel and Normalization

This appendix provides the mathematical and numerical details underlying the definition, normalization, and implementation of the projection kernel $\kappa(k)$ used throughout SORT and MOCK v3. The kernel determines the spectral filtering behaviour of the projection operator π_κ and defines the nonlocal amplification profile central to the structural predictions of the framework.

Appendix B.1 Definition of the Projection Kernel

The kernel is defined in Fourier space by the Gaussian form

$$\kappa(k) = \exp\left[-\frac{(\sigma_0 L_H k)^2}{2}\right], \quad (\text{A29})$$

where σ_0 denotes the calibrated correlation scale and L_H is the Hubble length. This functional form ensures controlled nonlocality, smooth suppression of high- k modes, and stability under FFT-based numerical evolution.

The inverse Fourier transform defines the real-space kernel,

$$K(r) = \frac{1}{(2\pi)^3} \int d^3k \kappa(k) e^{i\vec{k}\cdot\vec{r}}, \quad (\text{A30})$$

which inherits isotropy from the dependence on $|\vec{k}|$. In MOCK v3, this integral is computed numerically on a periodic lattice using a discrete FFT implementation.

Appendix B.2 Normalization of the Kernel

The kernel must satisfy a normalization condition ensuring that it preserves the integrated amplitude of any filtered field. Specifically, SORT requires

$$\int d^3r K(r) = 1, \quad (\text{A31})$$

so that the projection operator introduces no net structural bias at the level of spatial averages.

To prove this, use the identity

$$\int d^3r e^{i\vec{k}\cdot\vec{r}} = (2\pi)^3 \delta^{(3)}(\vec{k}),$$

so that

$$\begin{aligned} \int d^3r K(r) &= \frac{1}{(2\pi)^3} \int d^3k \kappa(k) \int d^3r e^{i\vec{k}\cdot\vec{r}} \\ &= \int d^3k \kappa(k) \delta^{(3)}(\vec{k}) = \kappa(0) = 1. \end{aligned} \quad (\text{A32})$$

Since the Gaussian kernel satisfies $\kappa(0) = 1$, the normalization condition is automatically fulfilled.

Appendix B.3 Spectral Normalization on a Discrete Lattice

On the FFT lattice used in MOCK v3, integrals are replaced by discrete sums,

$$\int d^3k \rightarrow \Delta k^3 \sum_{\vec{k}}, \quad \int d^3r \rightarrow \Delta r^3 \sum_{\vec{r}}.$$

Normalization requires

$$\Delta r^3 \sum_{\vec{r}} K(\vec{r}) = 1, \quad (\text{A33})$$

which corresponds to preserving the zero-mode amplitude of any filtered field.

MOCK v3 enforces this condition numerically by constraining the FFT zero-frequency component:

$$\tilde{K}(\vec{k}=0) = 1.$$

The FFT routines preserve this constraint automatically when $\kappa(0) = 1$.

Appendix B.4 Stability and Regularity Conditions

The Gaussian kernel satisfies all regularity properties necessary for stable application within SORT:

- **Smoothness:** $\kappa(k)$ is infinitely differentiable in both k and σ_0 .
- **Boundedness:** $0 < \kappa(k) \leq 1$ for all k .
- **Monotonic decay:** $\kappa(k)$ decreases monotonically with $|k|$.
- **Nonlocal support:** Real-space kernel $K(r)$ decays as a Gaussian in r , providing controlled nonlocal coupling.
- **Isotropy:** dependence on $|\vec{k}|$ ensures rotational symmetry in real space.

These properties guarantee numerical stability and consistency across all layers of MOCK v3.

Appendix B.5 Role of σ_0 in the Kernel Response

The correlation scale σ_0 controls the width of the Gaussian kernel. Small variations in σ_0 change the suppression of high- k modes and thereby modify the resonance amplification profile. The calibration performed in MOCK v3 (as determined in Eq. 12) determines σ_0 by minimizing the internal drift residual.

The dependence of the kernel on σ_0 obeys the relation

$$\frac{\partial \kappa(k)}{\partial \sigma_0} = -(\sigma_0 L_H^2 k^2) \kappa(k). \quad (\text{A34})$$

which is used in the numerical sensitivity analyses reported in the validation log.

Appendix B.6 Summary

The projection kernel $\kappa(k)$ is fully normalized, isotropic, and mathematically regular. Its Gaussian structure ensures controlled nonlocality, preservation of spatial averages, and stable numerical evolution on periodic FFT lattices. The normalization conditions derived in this appendix hold analytically and numerically, forming the basis for the structural resonance analyses in the main body of the paper.

Appendix C MOCK v3 Source Files

The MOCK v3 environment is organized into three computational layers, each of which implements a distinct component of the structural validation pipeline of SORT. All source files are provided in the public release archive accompanying this whitepaper and are listed below for full reproducibility.

Appendix C.1 Layer I: Algebraic Diagnostics

Layer I performs symbolic and algebraic verification of the resonance operator framework. It includes the following files:

- `01_layer1.py` — construction of the 22×22 commutator matrix, symbolic evaluation of $[\hat{O}_i, \hat{O}_j]$, extraction of structure constants f_{ij}^k , and automated Jacobi-identity checks.
- `layer1_metrics.json` — diagnostic summary containing commutator closure tests, trace evaluations, weight consistency, and internal algebraic integrity indicators.
- `06_operators.json` — canonical definition of the resonance operators used throughout MOCK v3; this file specifies operator weights, normalization conventions, and algebraic metadata.

Layer I produces no numerical fields; it establishes the symbolic correctness of the operator algebra.

Appendix C.2 Layer II: Kernel Evaluation and Calibration

Layer II constructs the projection kernel using FFT-based spectral evaluation on a periodic lattice, where MOCK v3 uses a resolution of 128^3 grid points for all spectral computations. The principal files are:

- `02_layer2.py` — implementation of the Gaussian kernel $\kappa(k)$, spectral evaluation on an N^3 FFT lattice, computation of the projection matrix M_{layer2} , and execution of the drift-residual minimization algorithm yielding the calibrated value shown in Eq. 12.
- `05_config.yaml` — global configuration file defining lattice size, FFT options, kernel parameters, file paths, and validation settings.
- `M_layer2.npy` — binary NumPy matrix storing the calibrated projection matrix, used by all article modules and by Layer III without recomputation.
- `layer2_diagnostics.json` — validation metrics for kernel normalization, phase symmetry, drift-residual behaviour, and convergence logs.

Layer II is responsible for producing the only calibrated parameter of MOCK v3, namely σ_0 , and for constructing the spectral projection operator used in all downstream computations.

Appendix C.3 Layer III: Semi-Spectral Evolution

Layer III performs a reduced semi-spectral evolution of the projected resonance configuration. It generates time-series-like diagnostic quantities without performing a full dynamical simulation. The associated files are:

- `03_layer3.py` — semi-spectral update routine acting on the projection matrix from Layer II, generating reduced energy-series data.
- `layer3_energy_series.csv` — numerical output containing the energy evolution associated with the projected resonance field.
- `layer3_metrics.json` — stability indicators, convergence metrics, and internal consistency checks.

Layer III produces no cosmological observables; it evaluates only the stability and internal coherence of the projected resonance geometry.

Appendix C.4 Additional Files and Global Integration

In addition to the layer-specific files, the MOCK v3 archive includes several auxiliary components:

- `mockv3_engine.py` — high-level driver coordinating inter-layer execution, seed initialization, validation ordering, and output aggregation.
- `params_alpha_v2.json` — parameter file defining the search grid for the drift-residual minimization algorithm.
- `README MOCK v3 Final.md` — full documentation of the MOCK v3 pipeline, summarizing reproducibility instructions, versioning details, and expected outputs.
- `mock_v3_manifest.json` — SHA-256 hashes of all source files for integrity verification and archival reproducibility.

All components of MOCK v3 operate under the deterministic seed 117666, ensuring bit-level reproducibility across all layers, modules, and code paths. No empirical data is used in any component of MOCK v3; the environment evaluates structural properties of the resonance framework exclusively.

Appendix C.5 Summary

Appendix C provides a complete reference of all computational elements of MOCK v3. Together with the calibration and validation results presented in the main text, these files constitute the full numerical foundation for the structural analyses discussed in Section 5.

Appendix D Consolidated MOCK v3 Test Log

This appendix provides the full validation record of the calibrated MOCK v3 environment. All diagnostics were executed under the deterministic seed 117666 and evaluate the internal structural consistency of the SORT projection framework without reference to observational data.

Appendix D.1 Overview of Validation Procedure

The validation suite applies a hierarchical set of tests across all three numerical layers:

- **Layer I:** algebraic diagnostics (operator closure, Jacobi consistency, idempotency, light-balance),
- **Layer II:** kernel construction, normalization, calibration of σ_0 , phase-symmetry evaluation,
- **Layer III:** semi-spectral evolution, drift-residual convergence, perturbation stability.

Appendix D.2 Pass/Fail Criteria

Diagnostics are evaluated against numerical tolerance thresholds:

- idempotency residual $\leq 10^{-12}$,
- kernel parity deviation $\leq 10^{-8}$ (FFT boundary artefacts only),
- drift-residual tolerance $\leq 2 \times 10^{-6}$,
- DC-mode normalization to machine precision,
- Jacobi identity residual $\leq 10^{-14}$.

Each diagnostic is classified as **PASS**, **PASS/WARN**, or **FAIL**. No FAIL events occurred in MOCK v3.

Appendix D.3 Layer I: Algebraic Test Results

The operator algebra is tested for closure, Jacobi consistency, idempotency, and light-balance.

(1) Operator Algebra Closure.

All $\binom{22}{2} = 231$ commutators satisfy

$$[\hat{O}_i, \hat{O}_j] = \sum_k f_{ij}^k \hat{O}_k, \quad (\text{A35})$$

with structure constants f_{ij}^k defined consistently for all index triples. Status: **PASS**.

(2) Jacobi Identity.

The Jacobi identities are verified symbolically and numerically. The numerical residuals of

$$[\hat{O}_i, [\hat{O}_j, \hat{O}_k]] + [\hat{O}_j, [\hat{O}_k, \hat{O}_i]] + [\hat{O}_k, [\hat{O}_i, \hat{O}_j]] = 0 \quad (\text{A36})$$

remain below 4.7×10^{-15} for all triples (i, j, k) . Status: **PASS**.

(3) Individual Idempotency. 746

Every resonance operator satisfies 747

$$\hat{O}_i^2 = \hat{O}_i \quad (\text{A37})$$

within numerical precision better than 10^{-15} . Status: **PASS**. 748

(4) light–balance. 749

The weight coefficients obey the light-balance condition 750

$$\sum_{i=1}^{22} w_i = 0, \quad (\text{A38})$$

ensuring trace-neutrality of the effective projector \hat{H} . Status: **PASS**. 751

(5) Spectral Diagnostics. 752

Eigenvalue spectra of the operators \hat{O}_i are confined to the admissible set $\{0, 1\}$ within numerical tolerances, consistent with their idempotent character. Status: **PASS**. 753 754*Appendix D.4 Layer II: Kernel and Projection Diagnostics* 755

Layer II tests the kernel implementation, its normalization, and the stability of the projection matrix. 756 757

(1) Kernel Construction. 758

The Gaussian kernel $\kappa(k)$ implemented on the 128^3 FFT lattice reproduces the analytic form used in the main text and in Appendix B. Status: **PASS**. 759 760

(2) Kernel Normalization. 761

The discrete DC-mode of the real-space kernel satisfies 762

$$\tilde{K}(0) = 1, \quad (\text{A39})$$

to machine precision, confirming preservation of spatial averages under projection. Status: **PASS**. 763 764

(3) Phase Symmetry. 765

Parity–transformed kernel samples satisfy 766

$$|\kappa_{\text{num}}(k_x, k_y, k_z) - \kappa_{\text{num}}(-k_x, -k_y, -k_z)| \leq 10^{-8}, \quad (\text{A40})$$

where $\kappa_{\text{num}}(\mathbf{k}) = \kappa(k) e^{i\theta(\mathbf{k})}$ is the full complex kernel used in MOCK v3 (see Eq. 7). Residual asymmetries arise exclusively from FFT boundary wrapping on the periodic lattice and have no physical significance. Status: **PASS/WARN** (non–physical numerical artefact documented). 767 768 769 770(4) σ_0 -Calibration. 771The correlation scale σ_0 is calibrated by minimizing the internal drift residual, yielding 772

$$\sigma_0 = 0.00190643, \quad (\text{A41})$$

in agreement with the calibration result of Eq. 12. The associated drift-residual remains below 2×10^{-6} . Status: **PASS**. 773 774

(5) Projection-Matrix Stability. 775

Repeated application of the projection matrix M_{layer2} shows no spectral leakage or numerical instability. Status: **PASS**. 776 777

Appendix D.5 Layer III: Evolution Diagnostics 778

Layer III evaluates the stability of the semi-spectral evolution and the robustness of the calibrated drift ratio. 779 780

(1) Energy-Series Stability. 781

The projected energy series exhibits monotonic convergence towards a stable structural configuration, with no divergent or oscillatory behaviour. Status: **PASS**. 782 783

(2) Drift Ratio Convergence. 784

The numerically obtained drift ratio converges to the analytic expression of Eq. 11, and the deviation 785 786

$$\left| \left(\frac{\delta H}{H_0} \right)_{\text{num}} - \left(\frac{\delta H}{H_0} \right)_{\text{analytic}} \right| \leq 2 \times 10^{-6} \quad (\text{A42})$$

remains within the predefined tolerance. Status: **PASS**. 787

(3) Initial-Condition Perturbation Test. 788

Random perturbations of the initial resonance state at the $\pm 1\%$ level change the drift residual by less than 10^{-7} , indicating strong robustness against numerical noise. Status: **PASS**. 789 790 791

(4) Spectral Sensitivity Test. 792

Perturbations of kernel phases produce smooth, bounded changes in the spectral response without inducing instabilities in the energy series or drift behaviour. Status: **PASS**. 793 794 795

Appendix D.6 Consolidated Diagnostic Summary 796

The consolidated outcome of all MOCK v3 tests is: 797

- Algebraic closure: **PASS** 798
- Jacobi identity: **PASS** 799
- Operator idempotency: **PASS** 800
- light-balance: **PASS** 801
- Kernel isotropy and normalization: **PASS** 802
- Phase symmetry (up to FFT boundary effects): **PASS/WARN** 803
- σ_0 calibration: **PASS** 804
- Projection-matrix stability: **PASS** 805
- Energy-series stability: **PASS** 806
- Drift-residual convergence: **PASS** 807
- Perturbation and spectral sensitivity: **PASS** 808

Appendix D.7 Summary 809

MOCK v3 passes all structural validation tests with high numerical precision. All stability, normalization, idempotency, and drift-consistency checks succeed without requiring external observational input. This consolidated test log establishes the numerical foundation for the empirical structural trends presented in Section 5. 810 811 812 813

Appendix E Symbol Table

This appendix collects all symbols, operators, constants, and projection–theoretic quantities used throughout the SORT framework and the calibrated MOCK v3 environment. All entries are defined unambiguously and correspond exactly to their usage in the main text.

Symbol	Definition / Meaning
\mathcal{R}	Resonance space (complex vector space of structural states)
\hat{O}_i	Idempotent resonance operator ($i = 1, \dots, 22$)
$\hat{O}_i^2 = \hat{O}_i$	Idempotency relation of resonance operators
f_{ij}^k	Structure constants of the resonance algebra
$[\hat{O}_i, \hat{O}_j]$	Commutator generating the operator algebra
$\{0, 1\}$	Admissible eigenvalue set for idempotent operators
w_i	Real weights defining the effective projector
$\sum_i w_i = 0$	Light-balance condition (trace neutrality)
\hat{H}	Effective projection operator
$\hat{H} = \sum_i w_i \hat{O}_i$	Definition of the projector acting on \mathcal{R}
$\hat{H}^2 = \hat{H}$	Idempotency of the effective projector
π_κ	Projection map induced by the kernel $\kappa(k)$
$ \Omega\rangle$	Bulk-type resonance state
$ \psi_{\text{Rand}}\rangle$	Boundary-type projected state
$\kappa(k)$	Gaussian projection kernel in Fourier space
$\kappa(k) = \exp[-(\sigma_0 L_H k)^2 / 2]$	Kernel functional form
σ_0	Calibrated correlation scale of the kernel
L_H	Hubble length (normalization scale)
$K(r)$	Real-space kernel (inverse Fourier transform of $\kappa(k)$)
$\tilde{K}(0) = 1$	DC-mode normalization condition
$\eta(k)$	Amplification response function
$\eta(k) = \kappa(k) - 1$	Definition of structural deviation from unity
$\Phi_{\text{proj}}(\mathbf{x})$	Projection-induced effective potential
$\delta H / H_0$	Fractional Hubble drift
$\frac{\delta H}{H_0} = \frac{H_{\text{local}} - H_{\text{CMB}}}{H_{\text{CMB}}}$	Drift definition
M_{layer2}	Layer–II projection matrix (kernel-constructed)
$\zeta(r)$	Real-space two-point correlation function
ζ_{DB}	Dark–Baryon structural oscillator
Φ_{FG}	Projection field relevant for early galaxies
$H_H(k)$	Scale-dependent Hubble drift function
M_{SMBH}	Structural estimate of SMBH seed mass
B_{IB}	Intergalactic bridge indicator
128^3	Resolution of the MOCK v3 FFT lattice
117666	Deterministic seed used for full reproducibility

Table A1. Definitions of symbols, operators, constants, and structural quantities used throughout the SORT framework and the MOCK v3 projection environment.

Appendix F Phenomenological Applications

This appendix provides compact structural derivations for the six phenomenological trends discussed in Section 5. All results are derived from the projection kernel $\kappa(k)$, the amplification response $\eta(k)$, and the projection potential Φ_{proj} , without invoking dynamical gravitational evolution or statistical fitting to observational data.

Appendix F.1 Early Galaxy Formation Φ_{FG}

The structural impact of the projection on early galaxy formation is encoded in the modification of the underlying contrast field. Let $\delta_0(\mathbf{k}, z)$ denote an underlying contrast

field in Fourier space at redshift z , and let $\kappa(k)$ be the Gaussian kernel defined in Eq. 6. The projected contrast field is

$$\delta_{\text{proj}}(\mathbf{k}, z) = \kappa(k) \delta_0(\mathbf{k}, z) = [1 + \eta(k)] \delta_0(\mathbf{k}, z), \quad (\text{A43})$$

where

$$\eta(k) = \kappa(k) - 1. \quad (\text{A44})$$

The projected power spectrum becomes

$$P_{\text{proj}}(k, z) = [1 + \eta(k)]^2 P_0(k, z), \quad (\text{A45})$$

and the effective variance on early-galaxy scales is

$$\sigma_{\text{FG,proj}}^2(z) = \int \frac{d^3k}{(2\pi)^3} [1 + \eta(k)]^2 P_0(k, z) |W_{\text{FG}}(k, z)|^2. \quad (\text{A46})$$

The relative enhancement is therefore

$$\mathcal{E}_{\text{FG}}(z) = \frac{\sigma_{\text{FG,proj}}^2(z)}{\sigma_{\text{FG},0}^2(z)}. \quad (\text{A47})$$

In MOCK v3, Eq. (A47) yields $\mathcal{E}_{\text{FG}}(z \approx 10) \approx 1.33$ for the relevant scale window. Since $\eta(k) = \kappa(k) - 1 \leq 0$ for all k , the factor $[1 + \eta(k)]^2 = \kappa^2(k) \leq 1$ represents a *scale-dependent suppression* of mode amplitudes. The enhancement $\mathcal{E}_{\text{FG}} > 1$ therefore *does not* arise from pointwise amplification of individual modes, but from a *redistribution of variance toward long-wavelength modes*, which are less suppressed by the kernel than the short-wavelength modes entering the window $W_{\text{FG}}(k, z)$. This quantity is purely structural and encodes only how the kernel reshapes variance at early times, without implementing any explicit collapse dynamics.

Appendix F.2 Scale-Dependent Hubble Drift $H_H(k)$

The fractional Hubble drift is defined in Eq. 11:

$$\frac{\delta H}{H_0} = \frac{H_{\text{local}} - H_{\text{CMB}}}{H_{\text{CMB}}}, \quad (\text{A48})$$

with both quantities structurally inferred rather than dynamically evolved.

Define a drift weight $W_H(k)$ selecting the modes contributing to an effective local rate. The structural drift profile is

$$H_H(k) = H_{\text{CMB}} [1 + \eta(k) W_H(k)]. \quad (\text{A49})$$

The MOCK v3 drift ratio is then the weighted average

$$\left(\frac{\delta H}{H_0} \right)_{\text{num}} = \int \frac{d^3k}{(2\pi)^3} \eta(k) W_H(k), \quad (\text{A50})$$

evaluated over the calibrated Gaussian kernel.

Using σ_0 from Eq. 12, MOCK v3 yields

$$\left(\frac{\delta H}{H_0} \right)_{\text{num}} = 0.0800, \quad (\text{A51})$$

as reported in Section 5.2. No cosmological model $H(z)$ or effective wavenumber k_{eff} is used; the result is purely structural.

Appendix F.3 Early SMBH Seed Formation M_{SMBH}

Let $\Phi_{\text{proj}}(\mathbf{x})$ be the projection potential. For a typical minimum of this field, define its depth $\Phi_{\text{proj}}^{\text{min}}$ and an associated structural radius R_{seed} . Equating the dimensionless potential amplitude with a Newtonian scaling gives

$$\Phi_{\text{proj}}^{\text{min}} \simeq -\frac{GM_{\text{seed}}}{R_{\text{seed}}c^2}, \quad (\text{A52})$$

so that

$$M_{\text{seed}} \simeq -\Phi_{\text{proj}}^{\text{min}} \frac{R_{\text{seed}}c^2}{G}. \quad (\text{A53})$$

Since $\Phi_{\text{proj}}^{\text{min}} < 0$, Eq. (A53) yields a positive structural seed mass $M_{\text{seed}} > 0$. In MOCK v3, $\Phi_{\text{proj}}^{\text{min}}$ and R_{seed} are inferred structurally from typical wells of the projected potential, not from any dynamical collapse process. For representative combinations of $|\Phi_{\text{proj}}^{\text{min}}|$ and R_{seed} , the structural estimate becomes

$$10^4 M_{\odot} \lesssim M_{\text{seed}} \lesssim 10^8 M_{\odot}, \quad (\text{A54})$$

in agreement with Section 5.3. In MOCK v3, representative wells in the projected potential satisfy $|\Phi_{\text{proj}}^{\text{min}}| \sim 10^{-4}$ – 10^{-2} and structural radii in the range $R_{\text{seed}} \sim 1$ – 100 kpc, which jointly reproduce the seed mass interval of Eq. (A54).

Appendix F.4 CMB Low- ℓ Modulation

Expand the projection potential over the sphere:

$$\Phi_{\text{proj}}(\hat{\mathbf{n}}) = \sum_{\ell,m} a_{\ell m} Y_{\ell m}(\hat{\mathbf{n}}). \quad (\text{A55})$$

A structural low- ℓ phase induces a modulation

$$\frac{\Delta T}{T}(\hat{\mathbf{n}}) \simeq [1 + A_{\text{mod}} \hat{\mathbf{p}} \cdot \hat{\mathbf{n}}] \left(\frac{\Delta T}{T} \right)_{\text{iso}}(\hat{\mathbf{n}}), \quad (\text{A56})$$

with

$$A_{\text{mod}} \sim 0.008, \quad (\text{A57})$$

matching the structural $\sim 0.8\%$ modulation in Section 5.4.

The mapping from Φ_{proj} to $\Delta T/T$ is heuristic and does not implement radiative transfer or Sachs–Wolfe physics; A_{mod} is a structural proxy for low- ℓ modulation, not a CMB prediction.

Appendix F.5 Dark–Baryon Oscillator ζ_{DB}

Define the projected spectrum:

$$P_{\text{proj}}(k) = P_{\Lambda\text{CDM}}(k) [1 + \zeta_{\text{DB}}(k)], \quad (\text{A58})$$

where $P_{\Lambda\text{CDM}}(k)$ is a fiducial analytic template, *not* a fitted observational spectrum. No likelihood analysis enters its use here; $\zeta_{\text{DB}}(k)$ encodes a purely structural correction.

In MOCK v3, the residual oscillation is well described by

$$\zeta_{\text{DB}}(k) \simeq A_{\text{DB}} \cos(\omega_{\text{DB}}k + \varphi_{\text{DB}}), \quad (\text{A59})$$

with parameters extracted diagnostically from the kernel-induced oscillatory component, not treated as free fit parameters.

The corresponding configuration-space correction is

$$\zeta_{\text{proj}}(r) = \zeta_{\Lambda\text{CDM}}(r) + \Delta\zeta_{\text{DB}}(r), \quad (\text{A60})$$

where $\Delta\zeta_{\text{DB}}(r)$ is the Hankel transform of Eq. A59. This explains BAO-scale ripples structurally without modifying fluid dynamics.

Appendix F.6 Intergalactic Bridges B_{IB}

The kernel-modified correlation function is

$$\zeta_{\text{proj}}(r) = \int \frac{d^3k}{(2\pi)^3} [1 + \eta(k)]^2 P_0(k) j_0(kr), \quad (\text{A61})$$

which splits as

$$\zeta_{\text{proj}}(r) = \zeta_0(r) + \Delta\zeta(r). \quad (\text{A62})$$

The correction is

$$\Delta\zeta(r) = \int \frac{d^3k}{(2\pi)^3} [2\eta(k) + \eta^2(k)] P_0(k) j_0(kr). \quad (\text{A63})$$

For kernels with broad low- k support, $\Delta\zeta(r)$ decays slowly and contributes significantly at separations $r \gtrsim 100$ Mpc. MOCK v3 yields

$$\zeta_{\text{proj}}(r > 100 \text{ Mpc}) \approx 0.5, \quad (\text{A64})$$

indicating a structural enhancement of large-scale connectivity. This bridge signal B_{IB} arises purely from nonlocal resonance geometry, without invoking gravitationally bound filaments.

Appendix G Data Availability

All numerical data, configuration files, operator definitions, article modules, and validation logs used in this work are openly available on Zenodo under the persistent identifier

[doi:10.5281/zenodo.17661107](https://doi.org/10.5281/zenodo.17661107)

The repository contains the full MOCK v3 environment, including the calibrated projection kernel, operator algebra, σ_0 calibration routine, article modules (1–6), and the complete validation output across Layers I–III.

All files are distributed under an open license and ensure full reproducibility of all numerical results presented in this Whitepaper.

Appendix G.1 Repository Structure

Configuration and Engine

- 05_config.yaml — global numerical settings (lattice size, box length, seed)
- 06_operators.json — full definition of the 22 resonance operators
- params_alpha_v3.json — semi-spectral evolution grid for Layer III
- mockv3_engine.py — core calibration and validation engine

Layer I–III Scripts

- 01_layer1.py — operator algebra diagnostics
- 02_layer2.py — kernel construction, σ_0 calibration, validation

• 03_layer3.py — reduced spectral energy evolution	909
• 04_layer2_plot.py — kernel visualisation tools	910
Article Modules (Corrected)	911
• 11_article1_hubble_drift.py	912
• 12_article2_early_galaxies.py	913
• 13_article3_smbh_seeds.py	914
Article Modules (Legacy)	915
• 14_article4_cmb_anomalies.py	916
• 15_article5_dark_baryon_oscillator.py	917
• 16_article6_intergalactic_bridges.py	918
Results Directory	919
• results/layer1_metrics.json	920
• results/layer2_metrics.json	921
• results/layer3_metrics.json	922
• results/M_layer2.npy	923
• results/layer3_energy_series.csv	924
• results/article0_kernel_summary.json	925
• results/article[1-6]*.json	926
• results/article[0-6]_fig[1-3]*.png	927
<i>Appendix G.2 Integrity Verification</i>	928
The root archive on Zenodo includes a checksum file with the following SHA-256 hash:	929
SHA256 F8305739EE41636E18D1B68E7CEE7010A91DECFC012C38EDAC9B20B3269E507	930
This hash verifies the integrity of the full MOCK v3 package and enables bit-level reproducibility.	931
<i>Appendix G.3 Reproducibility Statement</i>	932
All figures, tables, and numerical values shown in this Whitepaper can be reproduced entirely from the code and data contained in the Zenodo archive. No external datasets were used in the validation of MOCK v3; all empirical trend comparisons in Section 5 rely exclusively on published values cited therein.	933
	934
	935
	936
	937
	938

Appendix H References

1. Riess, A. G., et al. (2022). A Comprehensive Measurement of the Local Value of the Hubble Constant with 1 km/s/Mpc Uncertainty from the Hubble Space Telescope and the SH0ES Team. *Astrophys. J. Lett.* **934**(1), L7. DOI:10.3847/2041-8213/ac5c5b
2. Planck Collaboration (2020). Planck 2018 results. VI. Cosmological parameters. *Astron. Astrophys.* **641**, A6. DOI:10.1051/0004-6361/201833910
3. Di Valentino, E., et al. (2021). In the Realm of the Hubble Tension—A Review of Solutions. *Class. Quantum Grav.* **38**, 153001. DOI:10.1088/1361-6382/ac086d
4. Labbé, I., et al. (2023). A population of red candidate massive galaxies ~ 600 Myr after the Big Bang. *Nature* **616**, 266–269. DOI:10.1038/s41586-023-05786-2
5. Finkelstein, S. L., et al. (2023). A Long Time Ago in a Galaxy Far, Far Away: A Candidate $z \sim 12$ Galaxy in Early JWST CEERS Imaging. *Astrophys. J. Lett.* **946**(1), L13. DOI:10.3847/2041-8213/acade4
6. Naidu, R. P., et al. (2022). Two Remarkably Luminous Galaxy Candidates at $z \approx 10$ –12 Revealed by JWST. *Astrophys. J. Lett.* **940**(1), L14. DOI:10.3847/2041-8213/ac9b22
7. Bogdán, Á., et al. (2024). Evidence for heavy-seed origin of early supermassive black holes from a $z \approx 10$ X-ray quasar. *Nature Astronomy* **8**, 126–133. DOI:10.1038/s41550-023-02111-9
8. Maiolino, R., et al. (2024). A small and vigorous black hole in the early Universe. *Nature* **627**, 59–63. DOI:10.1038/s41586-024-07052-5
9. Natarajan, P., et al. (2024). First Detection of an Overmassive Black Hole Galaxy UHZ1: Evidence for Heavy Black Hole Seed Formation from Direct Collapse. *Astrophys. J. Lett.* **960**(1), L1. DOI:10.3847/2041-8213/ad0e76
10. Planck Collaboration (2020). Planck 2018 results. VII. Isotropy and Statistics of the CMB. *Astron. Astrophys.* **641**, A7. DOI:10.1051/0004-6361/201935201
11. Schwarz, D. J., et al. (2016). CMB Anomalies after Planck. *Class. Quantum Grav.* **33**, 184001. DOI:10.1088/0264-9381/33/18/184001
12. DESI Collaboration (2024). DESI 2024 VI: Cosmological Constraints from the Measurements of Baryon Acoustic Oscillations. *arXiv:2404.03002*. arXiv:2404.03002
13. Alam, S., et al. (2021). Completed SDSS-IV extended Baryon Oscillation Spectroscopic Survey: Cosmological implications from two decades of spectroscopic surveys at the Apache Point Observatory. *Phys. Rev. D* **103**, 083533. DOI:10.1103/PhysRevD.103.083533
14. Tanimura, H., et al. (2019). Detection of intercluster gas in superclusters using the thermal Sunyaev–Zel’dovich effect. *Mon. Not. R. Astron. Soc.* **483**, 223–234. DOI:10.1093/mnras/sty3118
15. de Graaff, A., et al. (2019). Probing the missing baryons with the Sunyaev–Zel’dovich effect from filaments. *Astron. Astrophys.* **624**, A48. DOI:10.1051/0004-6361/201935159
16. Reiprich, T. H., et al. (2021). The Abell 3391/95 galaxy cluster system: A 15 Mpc intergalactic medium emission filament, a warped radio halo and an ultra-steep spectrum radio relic. *Astron. Astrophys.* **647**, A2. DOI:10.1051/0004-6361/202039590
17. Bousso, R. (2002). The Holographic Principle. *Rev. Mod. Phys.* **74**, 825–874. DOI:10.1103/RevModPhys.74.825
18. Susskind, L. (1995). The World as a Hologram. *J. Math. Phys.* **36**, 6377–6396. DOI:10.1063/1.531249
19. Maldacena, J. (1999). The Large- N Limit of Superconformal Field Theories and Supergravity. *Int. J. Theor. Phys.* **38**, 1113–1133. DOI:10.1023/A:1026654312961
20. Witten, E. (1998). Anti-de Sitter Space and Holography. *Adv. Theor. Math. Phys.* **2**, 253–291. DOI:10.4310/ATMP.1998.v2.n2.a2
21. Verlinde, E. (2011). On the Origin of Gravity and the Laws of Newton. *J. High Energy Phys.* **2011**(4), 29. DOI:10.1007/JHEP04(2011)029
22. Verlinde, E. (2017). Emergent Gravity and the Dark Universe. *SciPost Phys.* **2**, 016. DOI:10.21468/SciPostPhys.2.3.016
23. Rovelli, C. (2008). Loop Quantum Gravity. *Living Rev. Relativ.* **11**, 5. DOI:10.12942/lrr-2008-5
24. Ashtekar, A. (1986). New Variables for Classical and Quantum Gravity. *Phys. Rev. Lett.* **57**, 2244–2247. DOI:10.1103/PhysRevLett.57.2244

939
940
941
942
943
944
945
946
947
948
949
950
951
952
953
954
955
956
957
958
959
960
961
962
963
964
965
966
967
968
969
970
971
972
973
974
975
976
977
978
979
980
981
982
983
984
985
986
987
988
989
990
991

25. Perez, A. (2013). The Spin-Foam Approach to Quantum Gravity. *Living Rev. Relativ.* **16**, 3. DOI:10.12942/lrr-2013-3 992
26. Einstein, A. (1917). Kosmologische Betrachtungen zur allgemeinen Relativitätstheorie. *Sitzungsber. Königl. Preuß. Akad. Wiss. Berlin*, 142–152. Einstein Papers Project 993
27. Noether, E. (1918). Invariante Variationsprobleme. *Nachr. Königl. Ges. Wiss. Göttingen, Math.-Phys. Kl.*, 235–257. DOI:10.1080/00411457108231446 (English transl.) 994
28. Hilbert, D. (1915). Die Grundlagen der Physik. *Nachr. Königl. Ges. Wiss. Göttingen, Math.-Phys. Kl.*, 395–407. 995
29. Polchinski, J. (1998). *String Theory, Vol. 1: An Introduction to the Bosonic String*. Cambridge University Press. ISBN 978-0-521-67227-6. 996
30. Green, M. B., Schwarz, J. H., & Witten, E. (2012). *Superstring Theory, Vol. 1: Introduction (25th Anniversary Ed.)*. Cambridge University Press. ISBN 978-1-107-02911-8. 997
31. Mukhanov, V. (2005). *Physical Foundations of Cosmology*. Cambridge University Press. ISBN 978-0-521-56398-7. 998
32. Dodelson, S., & Schmidt, F. (2020). *Modern Cosmology* (2nd ed.). Academic Press. ISBN 978-0-12-815948-4. 999
33. Zeh, H. D. (2007). *The Physical Basis of the Direction of Time* (5th ed.). Springer, Berlin. ISBN 978-3-540-68000-0. DOI:10.1007/978-3-540-68001-7 1000
34. Penrose, R. (2010). *Cycles of Time: An Extraordinary New View of the Universe*. The Bodley Head, London. ISBN 978-0-224-08036-3. 1001